Electronic Supplementary Material (ESI) for Physical Chemistry Chemical Physics.

Monitoring Photo-induced Population Dynamics in Metastable Linkage Isomer Crystals: A Crystallographic Kinetic Study of $[Pd(Bu_4dien)NO_2]BPh_4$

Supplementary Information

Lauren E. Hatcher, Jonathan M. Skelton, Mark R. Warren, Clare Stubbs, E. Lora da Silva and Paul R. Raithby

S1. GS and MS structures of [1].THF

	GS: nitro-(η^1-$\underline{N}O_2$)		MS: nitrito-(η^1-$\underline{O}NO$)	
Irradiation time [s]	-		60	
Temperature [K]	100(2)		100(2)	
Empirical formula	$C_{48}H_{73}B_1N_4O_3Pd_1$		$C_{48}H_{73}B_1N_4O_3Pd_1$	
Formula weight [g mol^{-1}]	871.31		871.31	
Crystal system	Monoclinic		Monoclinic	
Space group	$P2_1/n$		$P2_1/n$	
Unit cell parameters [Å, °]	a = 11.5457(4) b = 13.4021(5) c = 29.7173(12)	α = 90 β = 95.355(4) γ = 90	a = 11.4775(4) b = 13.3647(5) c = 29.9849(8)	α = 90 β = 94.569(3) γ = 90
Volume [Å^3]	4578.4(3)		4584.9(3)	
Z	4		4	
Density (calculated) [M g m^{-3}]	1.264		1.262	
Absorption coefficient μ [mm^{-1}]	0.451		0.448	
F(000)	1856		1856	
R_{int}	0.0459		0.0661	
Completeness (to ϑ = 25°)	0.998		0.998	
R_1 (observed data)	0.0428		0.0428	
wR_2 (all data)	0.0863		0.0901	
Reflections (independent)	19627 (9335)		31062 (9355)	

Table S1 Single crystal X-ray data for the ground state (GS) and metastable state (MS) structures of [1].THF at 100K.[1]

S2. Circuit diagram of the LED setup.

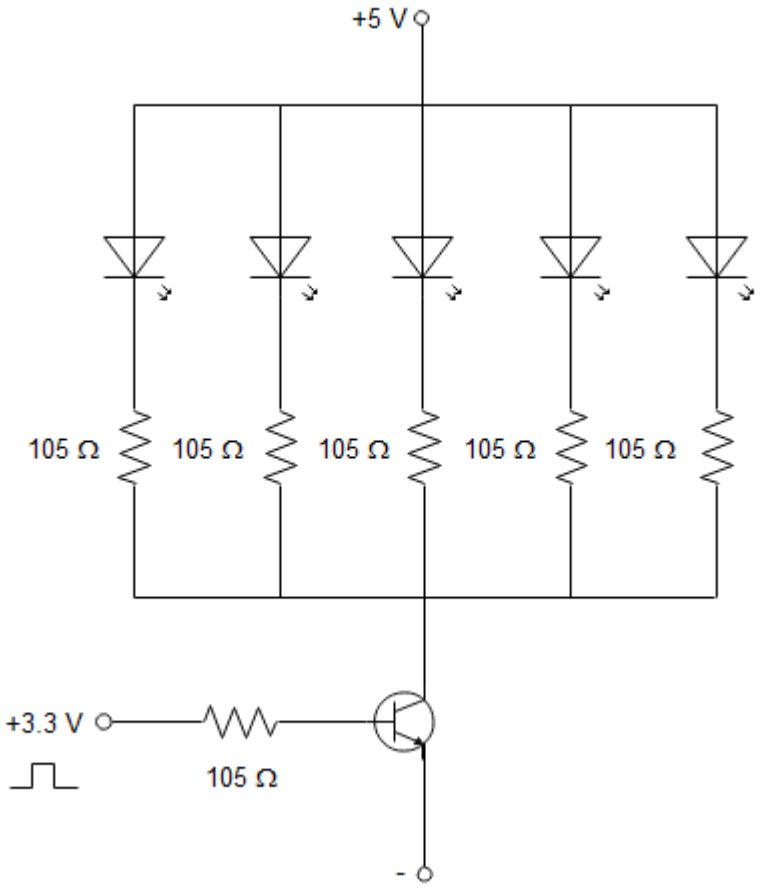

Figure S1 Circuit diagram for the LED illumination ring used in photocrystallographic studies on the laboratory measurement setup at the University of Bath. The LEDs are switched through a transistor connected to a function generator that outputs an 8 kHz square wave with variable duty cycle, which is used to control the LED brightness (fluence) and the illumination time.

S3. Preliminary tests of the effect of LED wavelength on photoconversion

A crystal of [1].THF was mounted on the diffractometer at 100 K, in the dark, and a GS data collection performed to confirm a 100 % nitro-(η^1-NO_2) isomer (i.e. 0 % photo-conversion). The crystal was then held at 100 K and irradiated with five 390 nm LEDs (Bivar UVTZ-390-15, λ_p = 390 ± 2.5 nm, 3.4 V, 15 mA, 20 mW), using the *in-situ* irradiation set-up described in the text, for a period of 120 s. After the irradiation period, a second set of X-ray data was collected and used to ascertain the level of photoactivation in the crystal.

This procedure was repeated for wavelengths of 395, 400, 405, 430, 465 and 500 nm. The same crystal was used in all experiments, and between runs the crystal was flash-warmed to room temperature, then flash-cooled back to 100 K to reset to 100 % occupation of the GS nitro-(η^1-NO_2) isomer. The observed MS occupations as a function of LED wavelength are shown in Fig. S2.

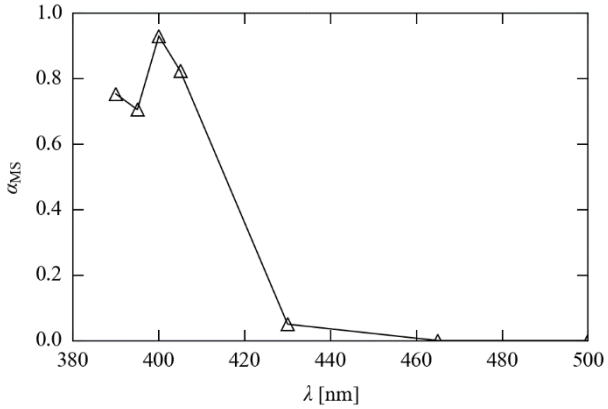

Figure S2 Occupation of the *endo*-nitrito-ONO MS isomer achieved in a single crystal of [1].THF following 120 s of irradiation with LED wavelengths in the range 390-500 nm at 100 K. The MS occupations were refined from full single-crystal X-ray data collections.

S4. Preliminary tests of the effect of crystal morphology on photoconversion

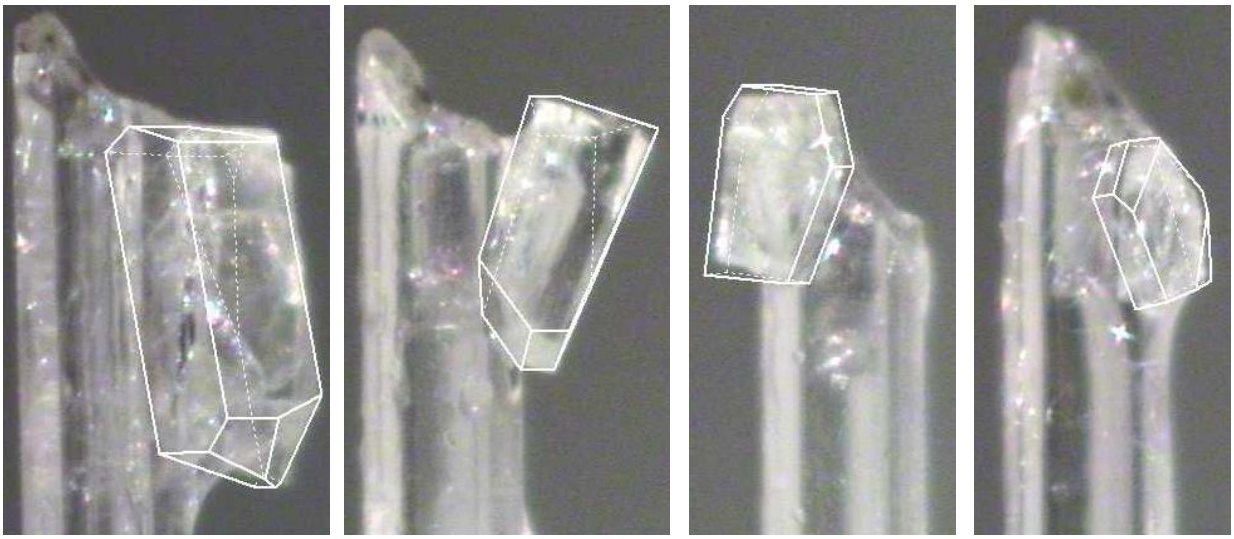

1 **2** **3** **4**

Figure S3 Microscope images of the four crystals used for the preliminary tests of the effect of crystal morphology on photoconversion. Crystals 1-4 are numbered by increasing A/V ratio, matching the points in Figure 4c in the text from left to right. All four images were obtained *in-situ* on the diffractometer under identical magnification. Crystal face indexing was performed using the Rigaku-Oxford Diffraction software CrysAlis Pro.[2]

S5. Derivation of photo-excitation profile with first-order kinetics and Beer-Lambert attenuation

To illustrate the ambiguity in interpreting the fitted JMAK parameters for photo-excitation curves, as highlighted in the text, we derive an alternative model for the metastable-state occupation as a function of time during a photo-excitation experiment, based on first-order kinetics and a Beer-Lambert attenuation of the light flux from the surface to the core of the crystal.

We begin by assuming a first-order excitation process (decay of the initial ground state) where the effective rate constant is given by the light intensity I and a constant k, i.e.:

$$\frac{\mathrm{d}\alpha_{\mathrm{GS}}}{\mathrm{d}t} = -Ik\alpha_{\mathrm{GS}} \qquad \text{Equation S1}$$

We next include a Beer-Lambert attenuation of the incident light from the surface to the centre of the crystal, i.e.:

$$I = I_0 e^{-\tau} \qquad \text{Equation S2}$$

The optical depth τ is related to the absorption coefficient of the transformed species, ε, and the path length through the transformed outer shells of the crystal l as $\tau = \varepsilon l$. Assuming the transformation proceeds homogenously from the surface into the bulk, for a spherical crystal with volume $V = \frac{4}{3}\pi r^3$ the path length through the converted outer shells is related to the fraction of unconverted volume remaining, i.e. α_{GS}, according to:

$$l = r\left[1 - (\alpha_{\mathrm{GS}})^{1/3}\right] \qquad \text{Equation S3}$$

Substituting Eq. S2 and S3 into Eq. S1 yields the following expression:

$$\frac{\mathrm{d}\alpha_{\mathrm{GS}}}{\mathrm{d}t} = -I_0 k\alpha_{\mathrm{GS}} e^{-\varepsilon r\left[1-(\alpha_{\mathrm{GS}})^{1/3}\right]} = -I_0 k\alpha_{\mathrm{GS}} e^{\varepsilon r(\alpha_{\mathrm{GS}})^{1/3}} e^{-\varepsilon r} \qquad \text{Equation S4}$$

Rearranging, we obtain the following integral:

$$\int \frac{1}{\alpha_{\mathrm{GS}}} e^{-\varepsilon r(\alpha_{\mathrm{GS}})^{1/3}} \mathrm{d}\alpha_{\mathrm{GS}} = \int -I_0 k e^{-\varepsilon r}\, \mathrm{d}t \qquad \text{Equation S5}$$

To integrate the left-hand side expression, we make the following substitution:

$$u = -\varepsilon r(\alpha_{GS})^{1/3} \rightarrow \frac{du}{d\alpha_{GS}} = -\frac{1}{3}\varepsilon r(\alpha_{GS})^{-2/3} \rightarrow d\alpha_{GS} = -\frac{3}{\varepsilon r}(\alpha_{GS})^{2/3} du \qquad \text{Equation S6}$$

This converts the integral to a form with a standard solution:

$$3\int \frac{1}{u} e^{u} du = 3\mathrm{Ei}(u) + C = 3\mathrm{Ei}\left(-\varepsilon r(\alpha_{GS})^{1/3}\right) + C \qquad \text{Equation S7}$$

where Ei is the exponential integral. Finally, integrating the right-hand side and simplifying gives the final expression:

$$\mathrm{Ei}\left(-\varepsilon r(\alpha_{GS})^{1/3}\right) = -\frac{1}{3} I_0 k e^{-\varepsilon r} t + \mathrm{Ei}(-\varepsilon r) \qquad \text{Equation S8}$$

where the constant of integration is obtained from the boundary condition that α_{GS} = 1 at t = 0.

Noting that $\alpha_{GS} = 1 - \alpha_{MS}$, and setting the constants ε, r, I_0 and k to 1 for simplicity, we plot the following for values of α_{MS} over the valid range of [0, 1]:

$$t = -3e\left\{\mathrm{Ei}\left(-(1 - \alpha_{MS})^{1/3}\right) - \mathrm{Ei}(-1)\right\} \qquad \text{Equation S8}$$

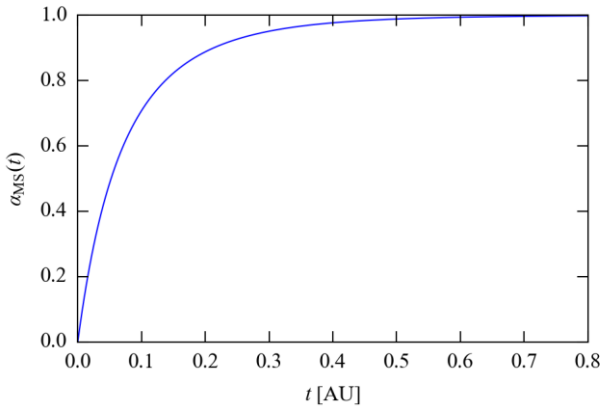

Figure S4 Plot of the function in Eq. S8. The time evolution of α_{MS} bears a remarkable resemblance to a JMAK curve (c.f. Fig. 5 in the text).

The curve in Fig. S4 bears a strong resemblance a JMAK profile, but clearly has a very different physical interpretation. Crucially, we see that in this model the illumination intensity and crystal morphology would be subsumed into the fitted JMAK parameters, which would make them directly dependent on the excitation

source, and also indirectly dependent on the X-ray source and detector *via* the restrictions the setup places on the crystal morphology.

The implications of this are that: (1) the JMAK parameters obtained from fitting the photo-excitation curves cannot be straightforwardly related to underlying molecular processes; and (2) to be predictive (e.g. for designing pump-probe X-ray diffraction experiments), our kinetic model would need to be parameterised with excitation data collected using the same setup. Regarding the latter, however, given the potential for other differences between setups, e.g. in temperature control, parameterising the model using data collected on the target setup should be considered standard protocol.

S6. Crystal packing

T [K]	Contact	D…A distance (esd) [Å]	H…A distance [Å]	DĤA angle [°]
100	C(16)-H(16A)…O(1)	3.728(4)	2.970	135.1
100	C(37)-H(37)…O(1)	3.502(4)	2.610	156.3
100	C(47)-H(47A)…O(1)	3.33(2)	2.696	135.1
100	C(10)-H(10B)…O(2)	3.633(4)	2.707	155.7
100	C(12)-H(12A)…O(2)	3.823(5)	3.073	134.5
100	C(37)-H(37)…O(2)	3.952(4)	3.064	156.1
200	C(16)-H(16A)…O(1)	3.863(6)	3.125	133.3
200	C(37)-H(37)…O(1)	3.534(5)	2.652	154.7
200	C(47)-H(47A)…O(1)	3.35(1)	2.627	130.2
200	C(10)-H(10B)…O(2)	3.719(5)	2.779	158.5
200	C(12)-H(12A)…O(2)	3.920(6)	3.190	132.8
200	C(37)-H(37)…O(2)	3.953(6)	3.050	159.4

Table S2 Bond distances and angles for C-H…O weak hydrogen bond interactions involving the nitro-(η^1-NO_2) ligand in GS structures of [1].THF at 100 and 200 K.

	Reaction cavity size		Reaction cavity size / Z	
T [K]	V [Å^3]	V [%]	V [Å^3]	V [%]
100	198.36	4.3	49.59	1.08
200	215.28	4.6	53.82	1.15

Table S3 Reaction cavity analysis for the GS structure of [1].THF at 100 and 200 K. Cavity volumes are calculated in Mercury [3] by deleting the photoactive group then performing a contact surface void space calculation (probe radius 1.2 Å, grid spacing 0.1 Å).

S7. Kinetic analysis of decay data collected at Diamond Light Source Beamline I19

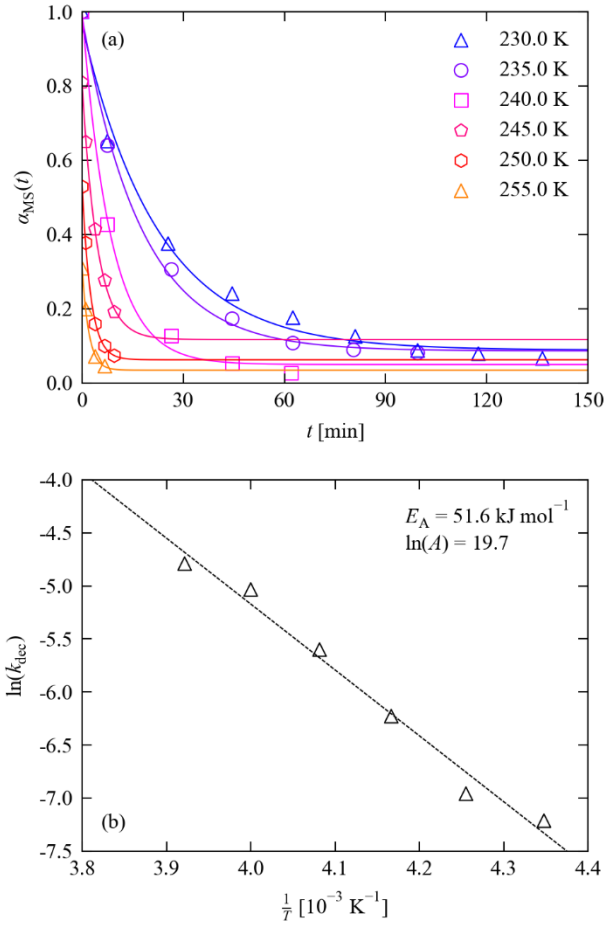

Figure S5 (a) Population of the metastable (MS) *endo*-nitrito-ONO form of [1].THF as a function of time during decay experiments performed using the synchrotron setup at temperatures from 230-255 K. The markers show the refined occupations, and the solid lines are fits to the JMAK model (Eq. 4 in the text) with the Avrami exponent n fixed to 1 (parameters given in Table S4). (b) Fit of the extracted decay rate constants to the Arrhenius expression (Eq. 5 in the text), with the fitting parameters as marked.

T [K]	α_{MS}^{0}	α_{MS}^{∞}	k [10^{-5} s^{-n}]	n	RMS [%]
230	0.96	0.09	73.63	1	3.09
235	0.98	0.09	94.93		1.74
240	1.00	0.05	197.3		1.99
245	0.80	0.12	369.5		0.75
250	0.53	0.06	651.0		0.44
255	0.31	0.03	831.0		0.20

Table S4 Fitted JMAK parameters of the decay curves in Fig. S4.

	$t_{x=0.5}$ [min]				
T [K]	Predicted	Laboratory	Δ [×]	Synchrotron	Δ [×]
212.5	324	235	1.38	-	-
215.0	217	199	1.09	-	-
217.5	147	159	0.93	-	-
220.0	101	111	0.91	-	-
230.0	23.9	40.0	0.60	15.2	1.57
235.0	12.2	-	-	13.1	0.93
240.0	6.38	-	-	6.37	1.00
245.0	3.44	-	-	2.86	1.20
250.0	1.90	-	-	2.05	0.92
255.0	1.07	-	-	1.55	0.69

Table S5 Predicted values of $t_{x=0.5}$ at the temperatures at which decay curves were measured using the laboratory and synchrotron setups compared to values estimated from experimental data. The predicted values were obtained using Eq. 7 in the text with the kinetic parameters from fitting the laboratory measurements with the Avrami exponent n fixed to 1. The estimates from the experimental data were made by using linear interpolation to find the time taken for the metastable-state population to reach $\alpha_{\mathrm{MS}} = \alpha_{\mathrm{MS}}^{0} - \frac{1}{2}(\alpha_{\mathrm{MS}}^{\infty} - \alpha_{\mathrm{MS}}^{0})$, and are therefore somewhat approximate. For each set of experimental measurements, the predicted $t_{x=0.5}$ values are within a factor of 2 of the estimated ones, corresponding to a temperature offset of < 10 K.

S8. Kinetic analyses with fitted Avrami exponent

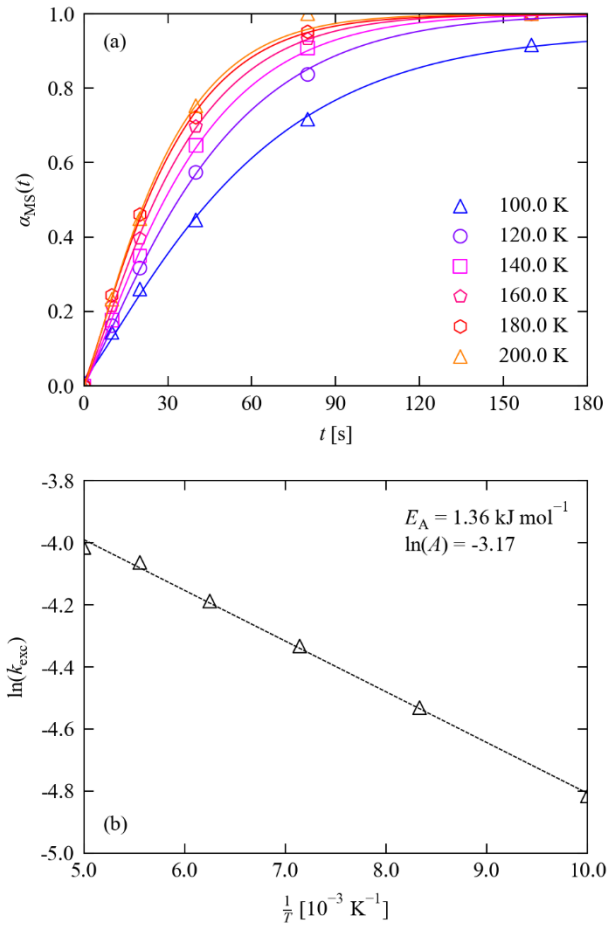

Figure S6 (a) MS population in [1].THF as a function of irradiation time at 100-200 K. Markers show the refined occupations, and solid lines indicate fits to the JMAK model (Eq. 4 in the text) with the Avrami exponent n allowed to vary (fitting parameters given in Table S6). (b) Fit of the extracted rate constants to the Arrhenius equation (Eq. 5 in the text), with parameters as marked.

T [K]	α_{MS}^{0}	α_{MS}^{∞}	k [10^{-2} s^{-n}]	n	RMS [%]
100	0.02	0.95	0.81	1.18	1.33
120	0.01	1.00	1.08		0.89
140	0.00	1.00	1.31		0.70
160	0.00	1.00	1.52		0.58
180	0.01	1.00	1.72		0.94
200	0.00	1.00	1.80		1.79

Table S6 Fitted JMAK parameters from the photo-excitation curves in Fig. S5.

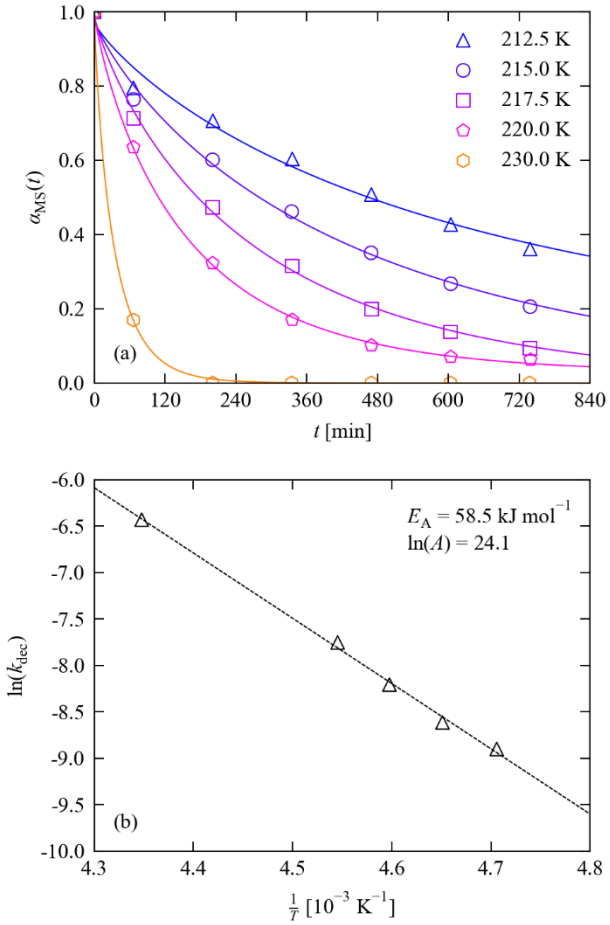

Figure S7 (a) MS population in [1].THF during decay studies performed at 212.5-230 K. Markers show the refined occupations, and solid lines indicate fits to the JMAK model (Eq. 4 in the text) with the Avrami exponent allowed to vary (fitting parameters in Table S7). (b) Fit of the extracted rate constants to the Arrhenius equation (Eq. 5 in the text), with parameters as marked.

T [K]	α_{MS}^{0}	α_{MS}^{∞}	k [10^{-5} s^{-n}]	n	RMS [%]
212.5	0.97	0.10	13.63		2.61
215.0	0.98	0.00	18.15		1.81
217.5	0.99	0.00	27.28	0.85	1.13
220.0	1.00	0.03	42.94		0.60
230.0	1.00	0.00	161.24		0.41

Table S7 Fitted JMAK parameters from the photo-excitation curves in Fig. S6.

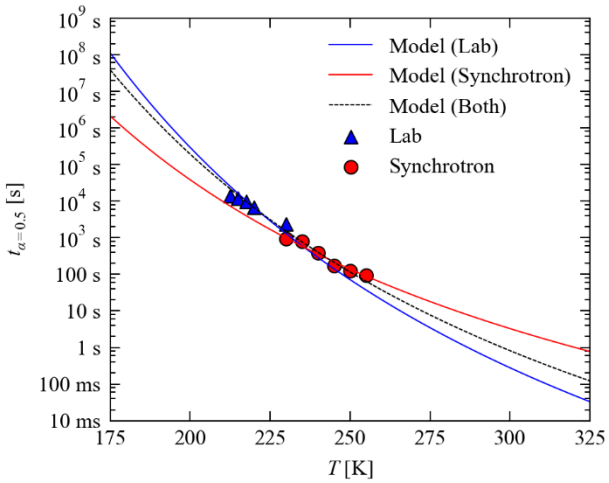

Figure S8 Predicted temperature dependence of the decay time $t_{x=0.5}$ as a function of temperature from 175-325 K. The blue and red lines show the predictions made from kinetic measurements conducted with the laboratory and synchrotron setups, respectively, while the dashed black line shows the predictions of a model incorporating both sets of data. The markers show values of $t_{x=0.5}$ estimated from the experimental measurements.

	$t_{x=0.5}$ [min]				
T [K]	Predicted	Laboratory	Δ [×]	Synchrotron	Δ [×]
212.5	361	235	1.54	-	-
215.0	241	199	1.21	-	-
217.5	162	159	1.02	-	-
220.0	110	111	0.99	-	-
230.0	25.3	40.0	0.63	15.2	1.67
235.0	12.8	-	-	13.1	0.97
240.0	6.61	-	-	6.37	1.04
245.0	3.52	-	-	2.86	1.23
250.0	1.92	-	-	2.05	0.94
255.0	1.07	-	-	1.55	0.69

Table S8 Predicted values of $t_{x=0.5}$ at the decay temperatures studied using the laboratory and synchrotron setups compared to estimates from experimental data. The predicted values were obtained using Eq. 7 in the text with the kinetic parameters from fitting the laboratory measurements with a variable Avrami exponent (see Tables S6 and S7). The estimates from the experimental data are approximate.

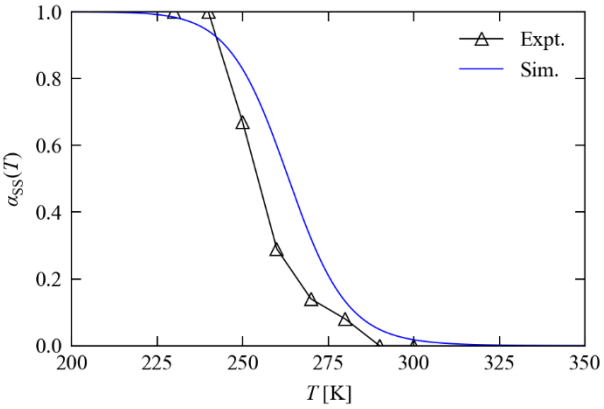

Figure S9 Steady-state occupations of the metastable state, α_{SS}, as a function of temperature. The predictions (blue lines) were made using numerical simulations with the kinetic parameters obtained from fitting the excitation and decay curves independently with variable Avrami exponents (see Tables S6 and S7).

S9. Comparison of the dynamic range $\Delta\alpha_{\mathrm{MS}}$ achievable with partial and complete excitation/decay

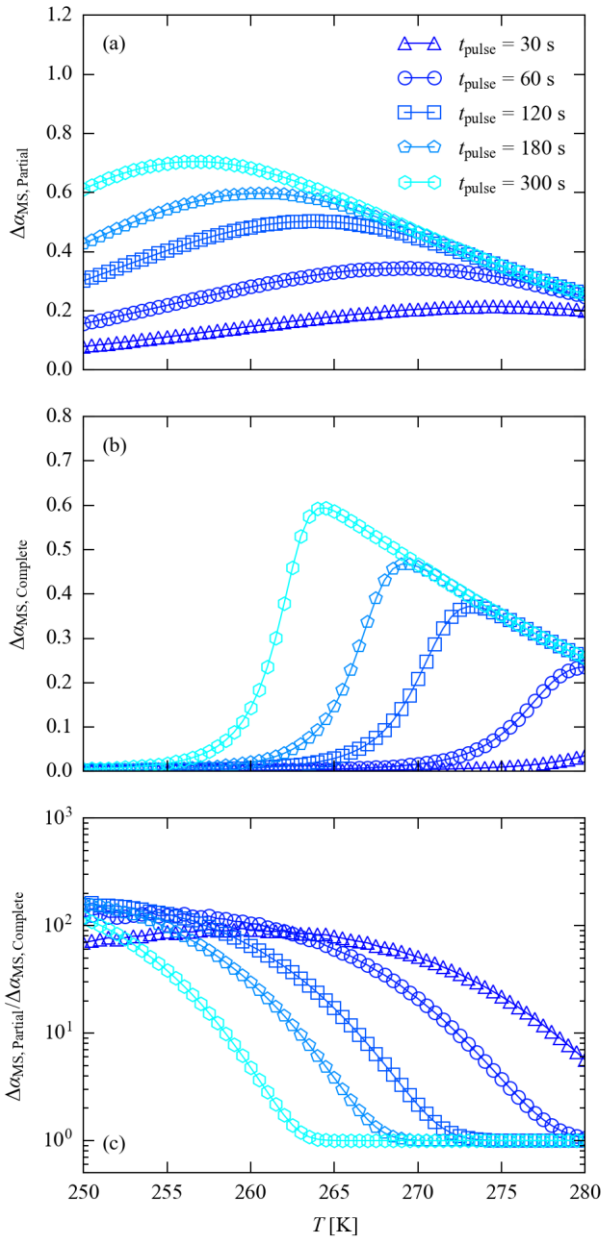

Figure S10 Optimised dynamic range in metastable-state occupation $\Delta\alpha_{\mathrm{MS}}$ between the initial and fully-pumped states in simulated pump-probe cycles with total pulse lengths of 30, 60, 120, 180 and 300 s. Plot (a) reproduces Fig. 11c in the text and shows the range achievable by allowing for incomplete excitation and decay. Plot (b) shows the range achievable within the constraint of complete decay (to $\alpha_{\mathrm{MS}} < 10^{-3}$) between cycles. Plot (c) shows the ratio between the ranges in (a) and (b) on a logarithmic scale.

S10. References

1. L. E. Hatcher, *CrystEngComm*, 2016, **18**, 4180-4187.
2. CrysAlis Pro, Rigaku Oxford Diffraction Data Collection and Data Reduction GUI, Version 171.38.43
3. C. F. Macrae, I. J. Bruno, J. A. Chisholm, P. R. Edgington, P. McCabe, E. Pidcock, L. Rodriguez-Monge, R. Taylor, J. v. d. Streek and P. A. Wood, *Journal of Applied Crystallography*, 2008, **41**, 466-470.